


Cite this: *RSC Adv.*, 2017, 7, 51079

# An arginine functionalized magnetic nano-sorbent for simultaneous removal of three metal ions from water samples†

Renu Verma,<sup>a</sup> Anupama Asthana,<sup>a</sup> Ajaya Kumar Singh<sup>\*a</sup> and Surendra Prasad <sup>\*b</sup>

The feasibility of using eco-friendly biodegradable arginine functionalized magnetic nanoparticle entrapped chitosan beads (AFMNPECBs) for simultaneous removal of three metal ions from water samples was evaluated under different conditions: concentration, pH, temperature and time. A novel approach was developed to synthesize AFMNPECBs for the removal of Cu(II), Co(II) and Ni(II) ions from aqueous solution. The synthesized AFMNPECBs were characterized by various techniques including Fourier transform infrared (FTIR), thermogravimetric analysis (TGA), vibrating sample magnetometer (VSM) and Brunauer–Emmett–Teller (BET). The adsorption kinetics study for Cu(II), Co(II) and Ni(II) ions on AFMNPECBs at pH 6 confirmed that it followed a pseudo second order kinetic model for all the metal ions. The adsorption isotherm data of the metal ions was fitted well with the Freundlich isotherm model. The maximum removal by AFMNPECBs was found to be 86, 82, and 71% and followed an order Cu(II) > Co(II) > Ni(II), respectively, with the maximum adsorption capacity being 172.4, 161.2, and 103.0 mg g<sup>-1</sup>, correspondingly. The AFMNPECBs exhibited highly effective adsorption for the removal of Cu(II), Co(II) and Ni(II) ions as they could be regenerated four times inexpensively by 0.1 M EDTA solution retaining 70% of the adsorption capacity.

Received 31st August 2017  
Accepted 17th October 2017

DOI: 10.1039/c7ra09705k

rsc.li/rsc-advances

## 1. Introduction

Heavy metals, naturally present in the environment, are among the most common environmental pollutants.<sup>1</sup> Several anthropogenic activities contribute a broad range of inorganic and organic emerging contaminants in wastewaters and the environment<sup>2</sup> where the quality of water is affected by contaminants like heavy metals being present at above the reference limits for human health and environmental protection.<sup>2,3</sup> Therefore, in recent years, extensive attention has been paid to management of the environment as well as water pollution caused by hazardous heavy metals as they pose severe threats to public health.<sup>4,5</sup>

Copper is an essential micronutrient in the human body as well as for aerobic life as it plays important physiological roles in many biological systems. However, like other heavy metals, it is potentially toxic, carcinogenic or fatal to human beings at high concentrations and prompts many serious diseases, such

as prion, Alzheimer's, Menkes and Wilson diseases,<sup>5,6</sup> and has been classified as one of the priority pollutants by US Environmental Protection Agency.<sup>5</sup> Nickel enters in the environment predominantly as a consequence of its several industrial uses while water and foods are the main source of Ni intake by human.<sup>7</sup> The exposure to Ni and its compounds cause serious problems, such as respiratory system cancer (carcinogenic), skin allergy and inhibit enzyme activity.<sup>7–9</sup> Cobalt is one of the essential oligo-element metals to the human body. Its toxic manifestations, however, have mainly been reported following its excessive inhalation targeting skin and respiratory tract and causes allergic dermatitis, rhinitis and asthma.<sup>10</sup> All these antagonistic properties of Cu, Ni and Co make it essential that their contents in air, water or food be determined regularly and where possible, removed.<sup>8</sup>

As a result of industrialization and rapid urbanization all over globe, the most common heavy metal ions found in industrial wastewater are Cu(II), Co(II) and Ni(II).<sup>11–14</sup> Therefore, a number of methods have been developed for the detection and removal of heavy metal ions from waste and drinking waters.<sup>1–8,12–19</sup> The traditional methods such as ion-exchange, chemical oxidation/reduction, chemical precipitation, ultra-filtration and reverse osmosis have several disadvantages such as high expense, prolonged period with less efficiency, production of other waste products, *etc.*<sup>19</sup> The adsorption method is still superior to other techniques because of its low-cost, simplicity of design, ease of operation, high effectiveness,

<sup>a</sup>Department of Chemistry, Government V.Y.T. Postgraduate Autonomous College, Durg, Chhattisgarh 491001, India. E-mail: [ajayaksingh\\_au@yahoo.co.in](mailto:ajayaksingh_au@yahoo.co.in); Fax: +91-788-2211688; Tel: +91-9406207572

<sup>b</sup>School of Biological and Chemical Sciences, Faculty of Science, Technology and Environment, The University of the South Pacific, Private Mail Bag, Suva, Fiji. E-mail: [prasad\\_su@usp.ac.fj](mailto:prasad_su@usp.ac.fj); Fax: +679-2321512; Tel: +679-3232416

† Electronic supplementary information (ESI) available. See DOI: 10.1039/c7ra09705k

reuse of the adsorbents along with their high adsorption capacity.<sup>2–5,12–16,19</sup> However, recent bias has been shifted to nanotechnology since nanoscale size, large surface area to volume ratio or efficiency, economic viability and environmental friendliness are all considered useful in the removal of heavy metal ions.<sup>12,19</sup>

Recently, magnetic nanoparticles (MNPs) have received attention as adsorbent for the effective removal of metal ions because they can be easily separated by external magnetic field after the adsorption process is completed.<sup>17,19</sup> However, bare MNPs are not applicable directly in adsorption process due to their strong dipole–dipole attraction between MNPs and high surface area may cause aggregation. Thus, polymer modified MNPs have been proved to be one of the most effective adsorbents due to different binding groups that target specific metal ions.<sup>17–19</sup> Chitosan, the most popular amino polysaccharide, having low cost, non-toxic, biodegradable, hydrophilic and highly reactive properties with metal ions because of the amino (–NH<sub>2</sub>) and hydroxyl (–OH) groups, has frequently been used for the removal of several metal ions.<sup>5,18,20–25</sup> However, poor chemical stability, low mechanical strength, separation and difficult recovery process are some significant drawbacks of chitosan.

The surface modified MNPs increases adsorption capacity of chitosan with high number of binding groups and thus has been used for As and Cr(vi) removal from aqueous solutions.<sup>26,27</sup> This entrapment of iron MNPs also improves mechanical separation process. Thus, a variety of chitosan derivatives have been developed such as Schiff base modified chitosan,<sup>28</sup> chitosan nanofibril,<sup>29</sup> chitosan immobilized on bentonite,<sup>30</sup> acrylamide grafted chitosan<sup>31</sup> and chitosan/magnetite composite beads<sup>21</sup> for the removal of different metal ions from aqueous solutions. Some modification of chitosan reduces the adsorption capacity due to wrapping binding groups where the number of nitrogen atoms in the chitosan do not remain enough.<sup>32</sup> Therefore, it is necessary to introduce high number of coordinating atoms onto the chitosan to enhance its adsorption capacity. There are very few reports where functionalized MNPs have been used for the removal of heavy metal ions.<sup>19,33,34</sup> The amino acid provides more functional groups which have strong affinity to bind heavy metal ions at the wide range of pH. Therefore, in continuation of our study on removal of the toxicants from water samples,<sup>19,35–37</sup> the present work was initiated with the objective to use AFMNPECBs for the simultaneous adsorptive removal of Cu(II), Co(II) and Ni(II) ions from aqueous solution. The kinetics and isotherm studies have also been investigated and discussed.

## 2. Materials and methods

### 2.1. Materials

Ferric chloride (FeCl<sub>3</sub>·6H<sub>2</sub>O), ferrous chloride (FeCl<sub>2</sub>·2H<sub>2</sub>O), HCl acid, ammonium hydroxide (NH<sub>4</sub>OH) and sodium hydroxide (NaOH) were purchased from Loba Chemie (Mumbai, India). Copper sulphate (CuSO<sub>4</sub>·5H<sub>2</sub>O), nickel sulfate (NiSO<sub>4</sub>·5H<sub>2</sub>O), cobalt nitrate (Co(NO<sub>3</sub>)<sub>3</sub>·6H<sub>2</sub>O), L-arginine were procured from Merck (Mumbai, India). All chemicals were of analytical grade and used as received. The solutions were prepared in double distilled water (DDW).

### 2.2. Equipment

The specific surface area of the adsorbent was determined by following Brunauer–Emmett–Teller (BET) method.<sup>36</sup> Nitrogen sorption isotherms were recorded on a BELSORP-mini II (BEL Japan, Inc.) at –196 °C (77 K). Pore size distribution of the adsorbent was recorded using BELSORP-mini II (BEL Japan, Inc.) involving Barrett–Joyner–Halenda (BJH) method. Fourier transform infrared spectra (FTIR) were recorded by a Fourier transform spectrophotometer (Perkin Elmer, USA, Frontier FT-IR/NIR) in absorbance mode with 32 scans for each sample. The thermogravimetric measurements were conducted in N<sub>2</sub> atmosphere (50 mL min<sup>–1</sup>) with a Hitachi thermo-gravimetry (EXSTAR TG-DTA 7200) at a heating rate of 10 °C min<sup>–1</sup>. Vibrating sample magnetometer (VSM, Lakeshore, model 7410) was used to determine the magnetization curve of the non-functionalized and functionalized adsorbents. The size of AFMNPs and AFMNPECBs were recorded using Zetasizer Nano ZS90 (ZEN3690, Malvern Instruments Ltd, UK) by dynamic light scattering (DLS) method. Surface morphology of AFMNPECBs at different magnification was studied by scanning electron microscope JEOL, JSM-6490LA Analysis Station, USA.

### 2.3. Preparation of arginine functionalized MNPs (AFMNPs)

The magnetic nanoparticles were prepared and modified with arginine. Briefly, 100 mL 0.3 M of FeCl<sub>3</sub>·6H<sub>2</sub>O and FeCl<sub>2</sub>·2H<sub>2</sub>O (mole ratio 2 : 1) were prepared, mixed well with magnetic stirrer. Then 1.5 M NH<sub>4</sub>OH was added drop wise into above mixed solution till pH 10 was reached. Initially solution turned to brown color and further addition of NH<sub>4</sub>OH gave black precipitate which indicated the formation of MNPs. NH<sub>4</sub>OH solution was added until precipitation completed. Then the solution with precipitate was stirred at 80 °C for 30 min and cooled to room temperature. There after the precipitate was separated by magnetic decantation and washed several times with DDW until the washings are neutral.<sup>20</sup> The separated MNPs were dispersed into 100 mL of 1% arginine solution, stirred for 1 h and then AFMNPs separated was by magnetic decantation and washed once again with DDW. The prepared AFMNPs were vacuumed dried at room temperature.<sup>34</sup>

### 2.4. Preparation of AFMNPECBs

The chitosan flakes 2 g were dissolved into 100 mL acetic acid solution. The viscous solution formed is left overnight for homogeneity. This was followed by the addition of 0.1 g of AFMNPs into the chitosan solution and mixed well. Then with the help of a syringe, 1 M NaOH solution was added drop wise which led to formation of the bead. The prepared beads were collected and washed with DDW until the pH of the washing became neutral. Then beads thus prepared were cross linked with glutaraldehyde (GLA) to form stable beads. The beads were suspended into 0.0938 mol L<sup>–1</sup> GLA solutions for 30 min with constant stirring. Finally, the AFMNPECBs were washed with DDW until pH of washing reached neutral. The beads were stored in DDW for further use. The systematic diagram for the synthesis of AFMNPECBs is shown in Fig. 1.



## 2.5. Adsorption experiment

All the experiments were performed by batch adsorption method using thermostat shaker water bath. For single system, a series Erlenmeyer flasks containing 0.1 g of adsorbent were immersed into thermostat with 10 mL of 100 mg L<sup>-1</sup> solutions of Cu(II), Co(II) and Ni(II) ions. For different batch of experiments, the concentrations of metal ions from 50–500 mg L<sup>-1</sup> were used. The mixture was shaken in water bath shaker at 30 °C. The effect of pH on the removal of metal ions was studied in the pH range 2–7. The adsorption isotherms studies for single system of Cu(II), Co(II) and Ni(II) ions were conducted at optimum pH 6. The Cu(II), Co(II) and Ni(II) ions were analyzed by UV-Visible spectrophotometer using sodium diethyl dithiocarbamate, potassium thiocyanate and dimethylglyoxime, respectively.<sup>38</sup> The percentage removal (*R*) and equilibrium adsorption capacity (*q<sub>e</sub>* mg L<sup>-1</sup>) and the kinetic adsorption capacity of metal ions were calculated using eqn (1), (2) and (3), respectively where *C<sub>o</sub>* and *C<sub>e</sub>* is the initial and equilibrium concentration of the metal ions (mg L<sup>-1</sup>), *C<sub>t</sub>* is the concentration of metal at time

*t*, *m* is the mass of the adsorbent (g) and *V* is the volume of the solution (mL).

$$R (\%) = \frac{C_o - C_e}{C_o} \times 100 \quad (1)$$

$$q_e = \frac{(C_o - C_e)V}{m} \quad (2)$$

$$q_t = \frac{C_o - C_t}{m} \times V \quad (3)$$

## 3. Results and discussion

### 3.1. Characterization of the adsorbent

The adsorption performance of adsorbent depends on its molecular structure as well as function groups. For the identification of existing functional groups the molecular structure of AFMNP and AFMNP/ECBs were analyzed using FTIR and their spectra are shown in Fig. 1S.† For AFMNP the bands at 588, 1644, 2924, 3425 cm<sup>-1</sup> were observed. The band at 588 cm<sup>-1</sup>

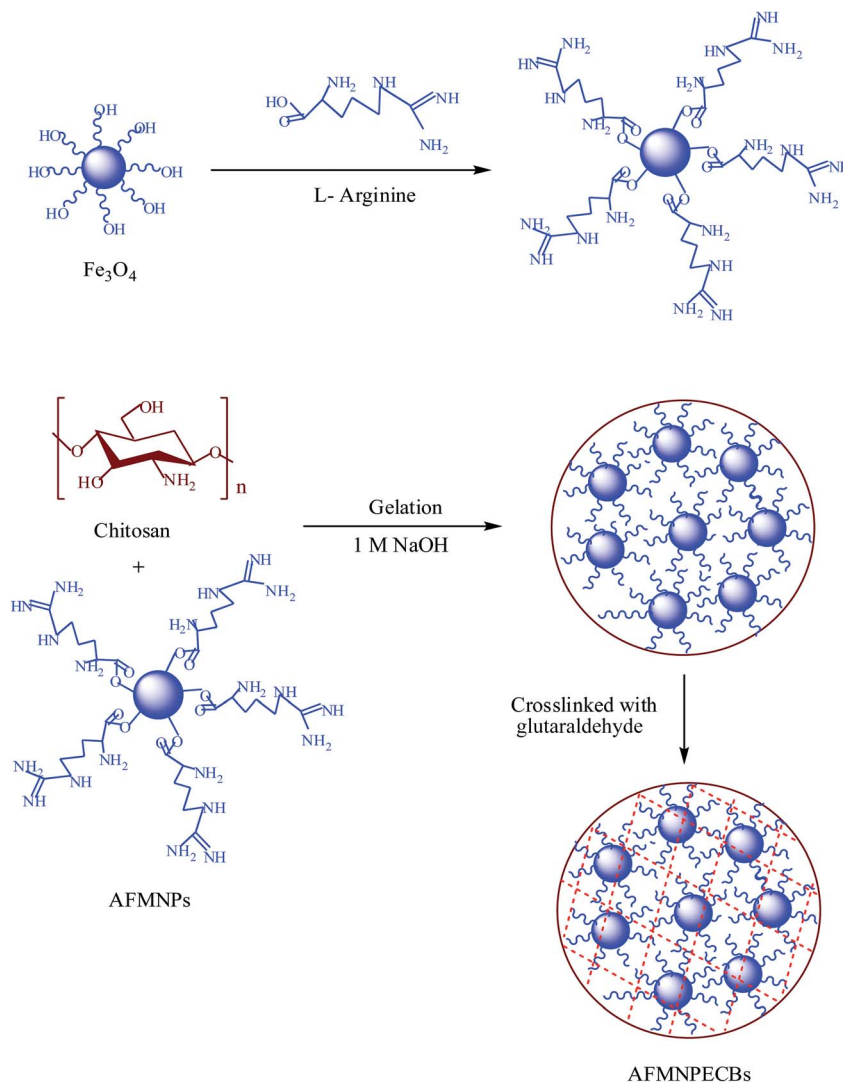


Fig. 1 The systematic diagram of arginine functionalized magnetic nanoparticle entrapped chitosan beads.



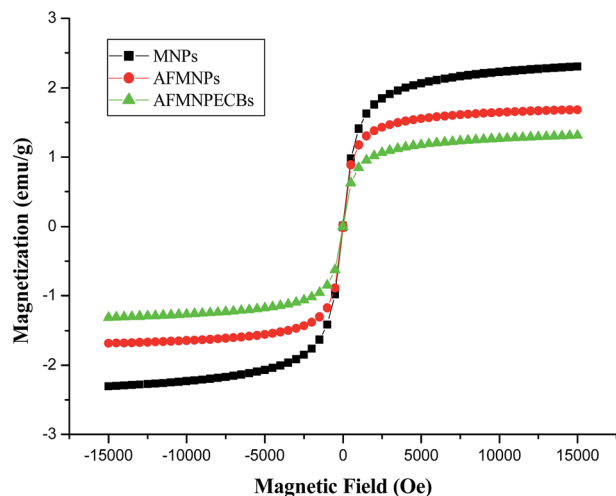


Fig. 2 Magnetization curves of non functionalized MNPs and functionalized AFMNPBs and AFMNPBECBs at room temperature.

attributed to Fe–O absorption while the band at  $2924\text{ cm}^{-1}$  was due to  $\text{--CH}$  stretching vibration. The sharp band at  $1644\text{ cm}^{-1}$  was due to the stretching vibration of  $\text{--C--CH}_2$  group and  $3425\text{ cm}^{-1}$  band indicated N–H stretching vibration. The presence of  $\text{--NH}_2$  and  $\text{--NH}$  groups demonstrated that arginine was successfully anchored onto the surface of MNPs.<sup>34</sup> In AFMNPBECBs, the characteristic band for Fe–O was at same  $588\text{ cm}^{-1}$  but new band at  $1370\text{ cm}^{-1}$  appeared due to  $\text{--NH}$  deformation vibration. Similarly, the band at  $1312\text{ cm}^{-1}$  indicated C–N amino group deformation and  $2924\text{ cm}^{-1}$  was due to  $\text{--CH}_2$  stretching vibration. The band at  $1649\text{ cm}^{-1}$  appeared due to  $\text{--NH}$  bending vibration in  $\text{--NH}_2$  while band at  $3440\text{ cm}^{-1}$  was due to  $\text{--OH}$  and  $\text{--NH}_2$  stretching vibrations. The band at  $1070\text{ cm}^{-1}$  was due to  $\text{--C--O}$  stretching vibration in  $\text{--C--OH}$ . The bands at  $1644$  and  $3425\text{ cm}^{-1}$  in AFMNPBs got shifted to higher wave numbers  $1649$  and  $3440\text{ cm}^{-1}$  in case of AFMNPBECBs. This shift confirmed that AFMNPBs are bonded with electrostatic attraction and hydrogen bonds in formation of AFMNPBECBs.

Fig. 2S† shows the DLS analysis for the size distribution of MNPs and AFMNPBs, the mean diameters of MNPs and AFMNPBs were found to be 217 and 853 nm, respectively. The increased

size of the AFMNPBs indicated the successful functionalization of MNPs by arginine.

The magnetic hysteresis curves for MNPs, AFMNPBs and AFMNPBECBs were recorded using VSM at room temperature and are provided in Fig. 2. The specific saturation magnetizations for MNPs, AFMNPBs and AFMNPBECBs were obtained at 2.3, 1.6 and  $1.3\text{ emu g}^{-1}$ , respectively. The saturation magnetization of AFMNPBs was reduced as MNPs functionalized by amino acid *i.e.* arginine. The saturation magnetization in case of AFMNPBECBs was also decreased due to entrapment of AFMNPBs into the chitosan. As the three prepared materials have strong magnetic properties so they could easily be removed from aqueous solution with the help of external magnetic field.

Fig. 3a–c shows the scanning electron microscopic (SEM) images of AFMNPBECBs at different magnification of 500, 1000, 10 000. These images clearly indicated the rough surface of AFMNPBECBs with the large surface areas. The BET surface area of AFMNPBECBs, shown in Fig. 3Sa and b,† calculated to be  $40.5\text{ m}^2\text{ g}^{-1}$  is higher than pure chitosan and chitosan derivatives *i.e.* have large surface area.<sup>29</sup> The total pore volume obtained  $0.189\text{ cm}^3\text{ g}^{-1}$  indicated mesoporous structure of AFMNPBECBs. The TEM images of AFMNPBECBs (Fig. 4) indicated to have spherical shape with average size  $12.83 \pm 1.91\text{ nm}$ . From high resolution TEM, the interfringe distance was measured to be 0.253, 0.209, 0.181 and 0.149 nm which corresponds to [311], [400], [422] and [440] plane of inverse spinel structured  $\text{Fe}_3\text{O}_4$ .

Thermogravimetric analysis (TGA) curves of MNPs, AFMNPBs and AFMNPBECBs are presented in Fig. 4S.† The TGA showed that there was no specific weight loss step in MNPs. At  $550^\circ\text{C}$  only 2% weight loss observed due to adsorbed water and bonded water. In case of AFMNPBs, 8% weight loss was observed which was due to degradation of amino acids functionalized on the surface of MNPs. However, the TGA curves of AFMNPBECBs showed considerable weight loss step at  $100^\circ\text{C}$  due to volatilization of adsorbed and bonded water. The second weight loss step observed at  $250\text{--}300^\circ\text{C}$  was due to degradation of chitosan. Finally, at  $550^\circ\text{C}$  AFMNPBECBs showed 50% weight loss. The TGA study confirmed that MNPs were successfully functionalized by arginine and AFMNPBs stay inside the polymer with enhanced thermal stability of AFMNPBECBs. The TGA study also explained the fact that

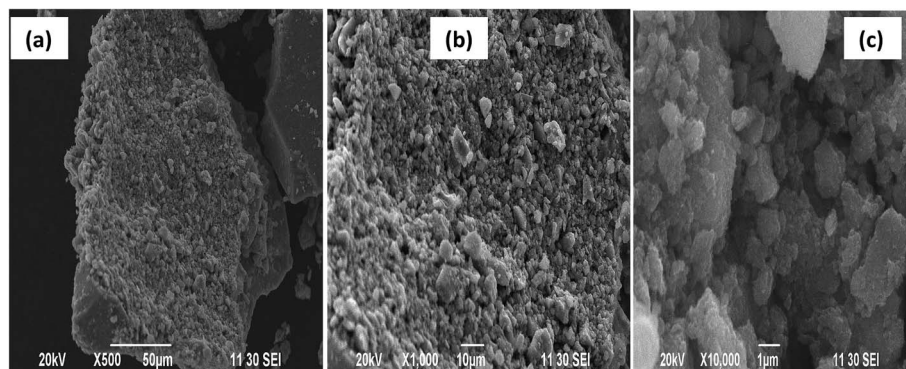


Fig. 3 SEM images of arginine functionalized magnetic nanoparticle entrapped chitosan beads (AFMNPBECBs) at different magnification (a) 500, (b) 1000 and (c) 10 000.





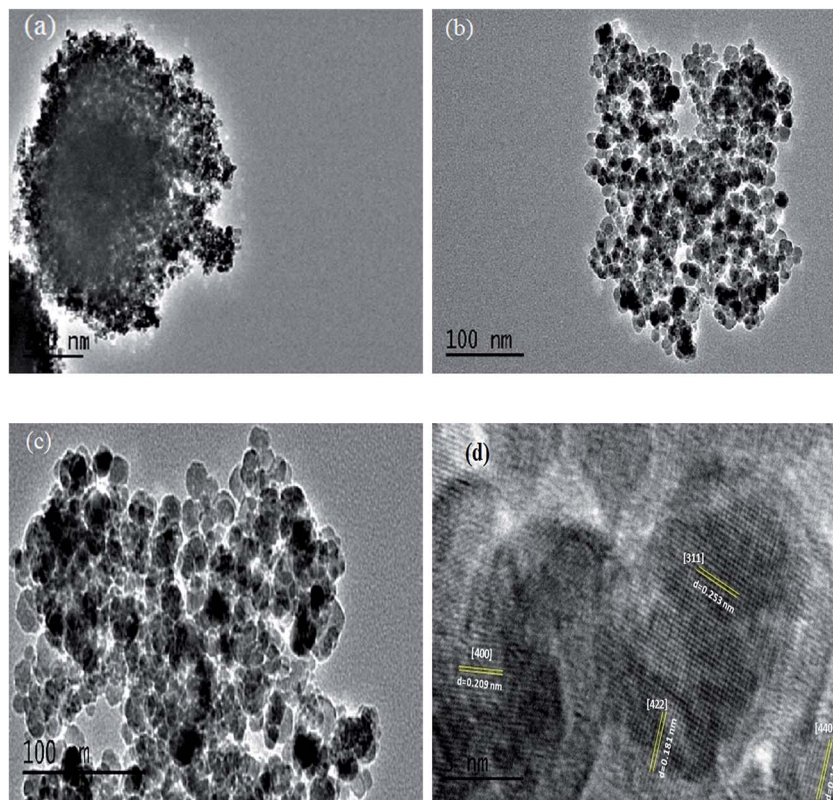


Fig. 4 TEM images of AFMNPECBs at different magnification (a) 250, (b) 100 (c) 100 and (d) 5 nm. The dark areas show  $\text{Fe}_3\text{O}_4$  MNPs while the light areas represent alginate polymer.

AFMNPs bind with chitosan by strong hydrogen as well as electrostatic bonds.

### 3.2. The effect of pH

The pH is a predominant parameter in adsorption process as the initial pH of the solution influences the adsorption capacity. Therefore, the effect of pH on the removal of three metal ions

was studied by varying pH from 2 to 7 and the results are shown in Fig. 5. It was observed that the adsorption capacity of the AFMNPECBs was the highest at pH 6 and followed the order  $\text{Cu(II)} > \text{Co(II)} > \text{Ni(II)}$ . The metal ions in the acidic medium are present cationic forms  $\text{M}^{2+}$  while in hydroxide forms in basic medium. Increasing of pH higher than 6, the metal ions start precipitating as insoluble hydroxides which reduced the concentration of free metal ions and thus decreased the removal capacity. At lower pH of the metal ions solution, amino group on the AFMNPECBs could be protonated and thereby induce electrostatic repulsion with the positively charged metal ions. In addition, the competition between  $\text{H}^+$  and metal ions also caused low adsorption. As pH was increased this increased the adsorption capacity of the AFMNPECBs. At pH 6, amino groups were un-protonated and easily donate lone pair of electron to metal ions to form complexes on the surface of adsorbent and thus showed the highest adsorption. The schematic representation of possible mechanism of adsorption of metal ions by AFMNPECBs is shown in Fig. 6.

### 3.3. Effect of time

The effect of contact time on the removal of  $\text{Cu(II)}$ ,  $\text{Co(II)}$  and  $\text{Ni(II)}$  ions by AFMNPECBs was studied up to 160 min. The effect of contact time was carried out taking 10 mL of  $100 \text{ mg L}^{-1}$  metal ions in conical flasks containing 0.1 g of adsorbent and the mixture was shaken at  $30^\circ\text{C}$ . As shown in Fig. 7, initially the uptake of metal ions by the adsorbent was quite high and

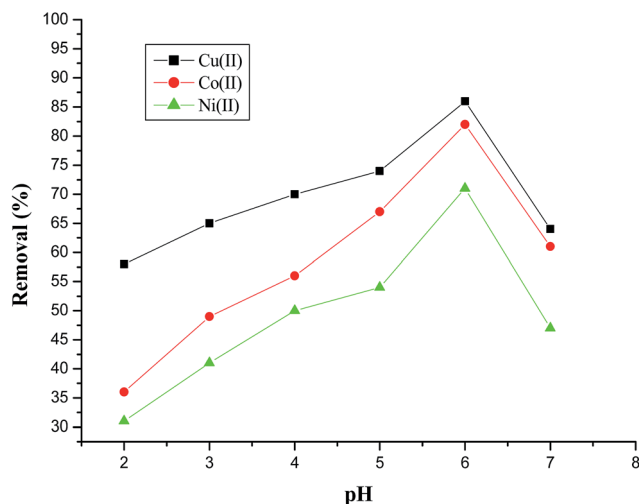


Fig. 5 Effect of pH on the removal of  $\text{Cu(II)}$ ,  $\text{Co(II)}$  and  $\text{Ni(II)}$  ions using AFMNPECBs at initial metal ions concentration  $100 \text{ mg L}^{-1}$ , contact time 160 min, adsorbent dose  $10 \text{ g L}^{-1}$  and temperature  $303 \text{ K}$ .



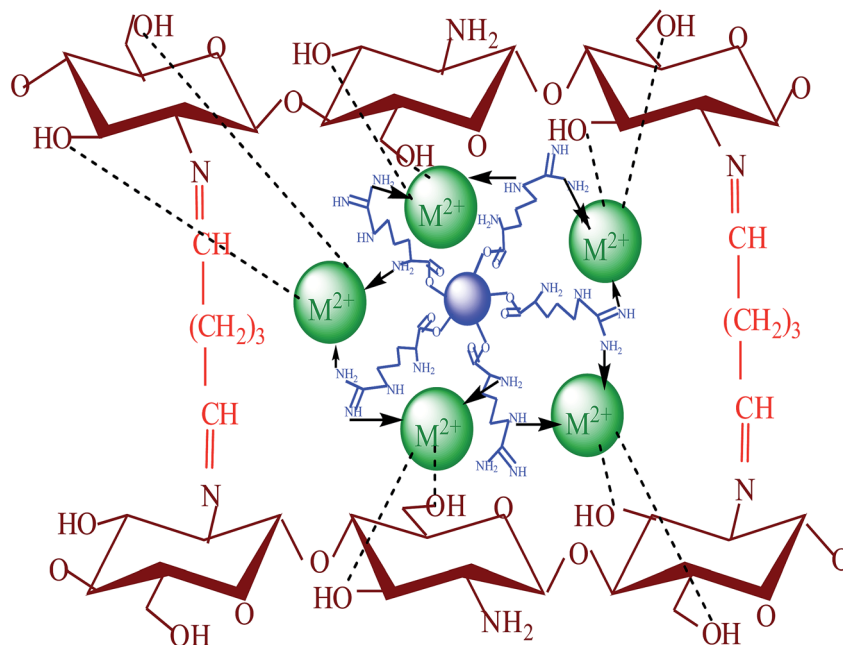


Fig. 6 The proposed mechanism of complexation of Cu(II), Co(II) and Ni(II) metal ions as  $M^{2+}$  on AFMNPECBs.

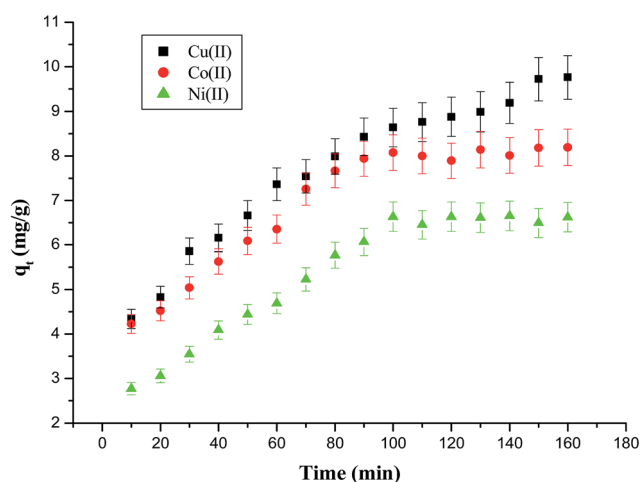


Fig. 7 The effect of contact time on the adsorption capacity of AFMNPECBs at initial metal ions concentration  $100 \text{ mg L}^{-1}$ , adsorbent dose  $10 \text{ g L}^{-1}$ , temperature  $303 \text{ K}$  and  $\text{pH } 6$ .

slowed down after around 100 min and gradually achieved equilibrium. The initial increased adsorption of metal ions was due to their rapid binding at the active sites of adsorbent in random manner. The rate of adsorption gradually decreased leading to equilibrium when adsorbent's active sites became saturated. The maximum percentage removal of Cu(II), Co(II) and Ni(II) ions was obtained as 86, 82 and 71%, respectively in 160, 90 and 100 min correspondingly.

### 3.4. The adsorption kinetics

The adsorption kinetic study provides important information on the rate and mechanism of adsorption. The study of the

effect contact time revealed that Cu(II), Co(II) and Ni(II) ions adsorption on AFMNPECBs showed two different phases: a rapid initial phase and a slow adsorption phase to reach equilibrium. Therefore, the adsorption kinetics of Cu(II), Co(II) and Ni(II) onto the AFMNPECBs was studied using different kinetics models whose linearized forms are shown in eqn (4), (5) and (6) as pseudo first order, pseudo second order<sup>19,39</sup> and intraparticle diffusion model<sup>19,40</sup> respectively.

$$\log(q_e - q_t) = \log q_e - \frac{k_1}{2.303} t \quad (4)$$

$$\frac{t}{q_t} = \frac{1}{k_2 q_e^2} + \frac{1}{q_e} t \quad (5)$$

$$q_t = K_{id} \sqrt{t} + A \quad (6)$$

here,  $q_e$  and  $q_t$  are the amount of Cu(II), Co(II) and Ni(II) ions per unit mass of the adsorbent *i.e.* adsorption capacity ( $\text{mg g}^{-1}$ ) at equilibrium at time  $t$  (min) and  $k_1$  ( $\text{min}^{-1}$ ) is the pseudo first order.  $k_2$  ( $\text{g mg}^{-1} \text{ min}^{-1}$ ) is the pseudo second order constant while  $A$  ( $\text{mg g}^{-1}$ ) is a constant and  $K_{id}$  ( $\text{mg g}^{-1} \text{ min}^{1/2}$ ) is diffusion rate constant of intraparticle diffusion model. The intraparticle diffusion model describes adsorption of metal ions on the adsorbent is completed by three stages as exterior surface adsorption, interior surface and equilibrium. In this model, the adsorption of metal ions firstly takes place at exterior surface then diffuses into interior pores where due to increasing resistance the diffusion rate is decreased. In the last stage, equilibrium is achieved because of very low concentration of metal ions in the solution.

The plots of  $\log(q_e - q_t)$  against  $t$  for pseudo first order,  $t/q_t$  against  $t$  for pseudo second order and  $q_t$  against  $t^{1/2}$  for intraparticle diffusion model for three metal ions are shown in



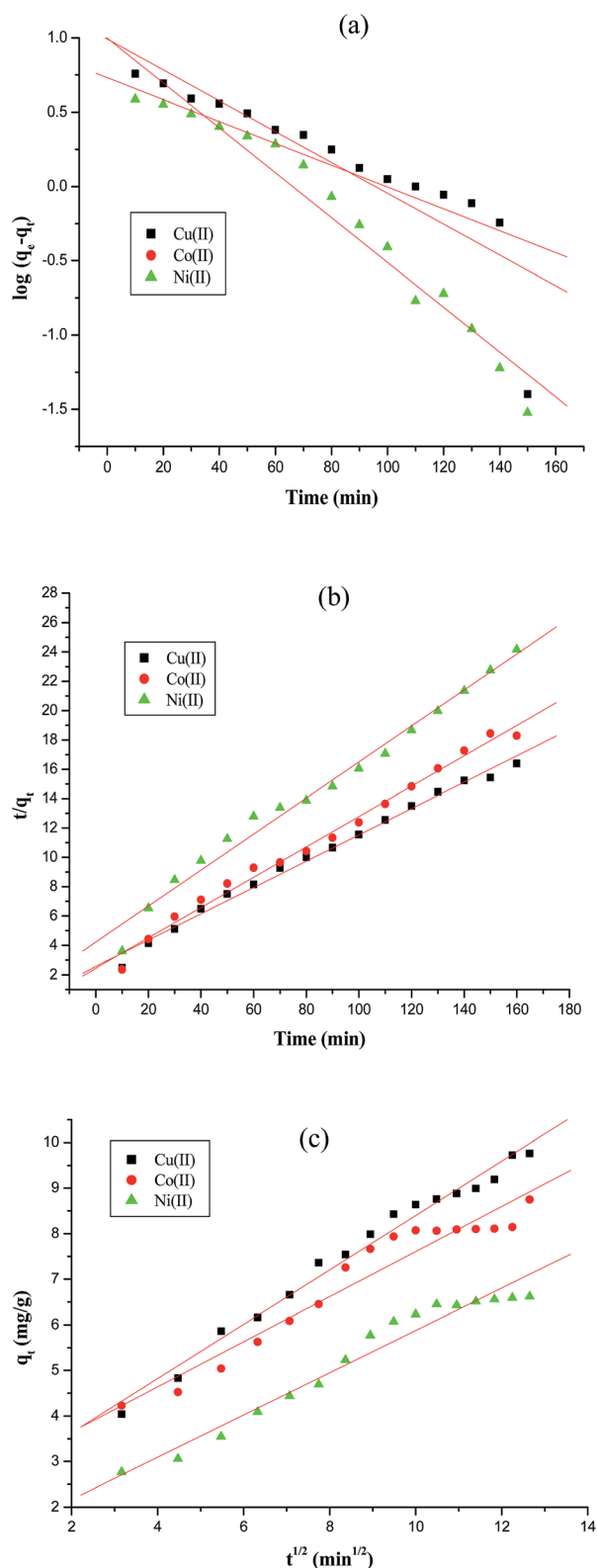


Fig. 8 Adsorption kinetics of Cu(II), Co(II) and Ni(II) ions on AFMNPECBs (a) pseudo first order (b) pseudo second order (c) intraparticle diffusion models at initial metal ions concentration  $100 \text{ mg L}^{-1}$ , temperature  $303 \text{ K}$ , contact time upto  $160 \text{ min}$ , adsorbent  $10 \text{ g L}^{-1}$  and pH 6.

**Table 1** Kinetic parameters for the adsorption of Cu(II), Co(II) and Ni(II) ions by AFMNPECBs under initial concentration  $100 \text{ mg L}^{-1}$ , contact time  $160 \text{ min}$ , adsorbent dose  $10 \text{ g L}^{-1}$ , temperature  $303 \text{ K}$  and pH 6

Kinetic models and parameters	Metal ions		
	Cu(II)	Co(II)	Ni(II)
<b>Pseudo first order</b>			
$k_1 \text{ (min}^{-1}\text{)}$	0.023	0.016	0.346
$q_e \text{ (mg g}^{-1}\text{)}$	9.794	5.370	9.931
$R^2$	0.765	0.922	0.952
<b>Pseudo second order</b>			
$k_2 \times 10^{-3} \text{ (g mg}^{-1} \text{ min}^{-1}\text{)}$	3.125	4.345	3.524
$q_e \text{ (mg g}^{-1}\text{)}$	11.23	9.708	8.196
$R^2$	0.991	0.989	0.984
<b>Intraparticle diffusion</b>			
$A \text{ (mg g}^{-1}\text{)}$	2.434	2.662	1.238
$K_{id} \text{ (mg g}^{-1} \text{ min}^{-1}\text{)}$	0.596	0.494	0.463
$R^2$	0.984	0.938	0.959

Fig. 8a, b and c, respectively. The values of the rate constants  $k_1$  and  $k_2$  for Cu(II), Co(II) and Ni(II) ions were calculated from the slopes of the plots of  $\log(q_e - q_t)$  versus  $t$  (Fig. 8a) and from the intercept of the linear plots of  $t/q_t$  versus  $t$  (Fig. 8b), respectively and reported in Table 1. The values of the diffusion constant  $K_{id}$  and constant  $A$  with respect to metal ions were also determined from the slope and intercept of the plots of  $q_t$  versus  $t^{1/2}$  (Fig. 8c), respectively as shown in Table 1.

The correlation coefficient ( $R^2$ ) values for three different metal ions along with kinetic parameters are also listed in Table 1. The Table 1 clearly shows that the correlation coefficients of pseudo second order are closer to 1 for all three metal ions and higher than those obtained in case of pseudo first order model. Thus, the adsorption of Cu(II), Co(II) and Ni(II) ions on AFMNPECBs perfectly followed with pseudo second order kinetics with  $R^2$  values 0.991, 0.989, and 0.984, respectively. This indicated that chemisorption was the rate controlling mechanism. The intraparticle diffusion model clearly showed two regions in the three plots for three metal ions with one break point as shown in Fig. 8c. These break points indicate that more than one process affected the adsorption of the metal ions *i.e.* two steps occurred during the adsorption. The first process was the diffusion of metal ions on the surface of the adsorbent and the second process was pore diffusion process leading to equilibrium. In no case, the straight lines passed through the origin indicated that the boundary layers diffusion of adsorbates also controlled the adsorption especially in case of intraparticle diffusion.<sup>18,19</sup> Furthermore, the  $R^2$  value in pseudo first order and intraparticle diffusion model for three metal ions are comparable which indicated that in addition to intraparticle diffusion some weak interaction is also involved in adsorption process.

### 3.5. Adsorption isotherms

The Langmuir and Freundlich adsorption isotherms have widely been used to determine the adsorption mechanism.<sup>19</sup>



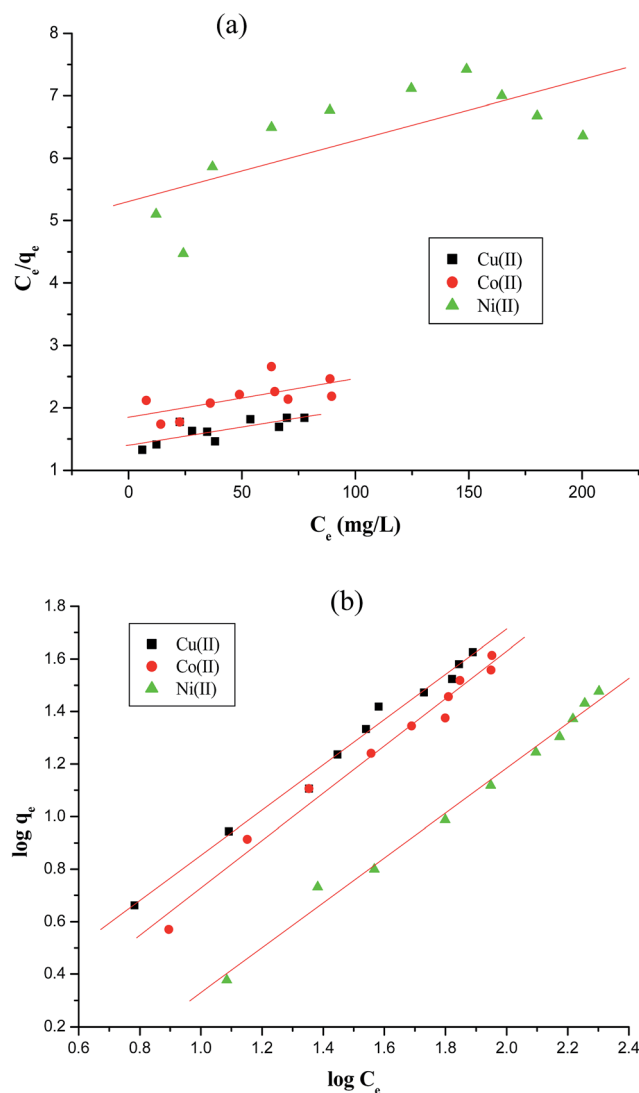


Fig. 9 Adsorption isotherms of Cu(II), Co(II) and Ni(II) ions on AFMN-PECBs (a) Langmuir (b) Freundlich model under the conditions given in Table 2.

The linear form of Langmuir and Freundlich models<sup>19,41</sup> can be expressed as given in eqn (7) and (8), respectively.

$$\frac{C_e}{q_e} = \frac{1}{K_L Q_m} + \frac{C_e}{Q_m} \quad (7)$$

$$\log q_e = \log K_F + (1/n) \log C_e \quad (8)$$

The  $C_e$  and  $q_e$  are the equilibrium concentration and adsorption capacity ( $\text{mg L}^{-1}$ ) of AFMNPECBs for Cu(II), Co(II) and Ni(II) ions.  $K_L$  is the Langmuir adsorption constant ( $\text{L mg}^{-1}$ ) and  $Q_m$  ( $\text{mg g}^{-1}$ ) is the maximum adsorption capacity at monolayer coverage ( $\text{mg g}^{-1}$ ).  $K_F$  ( $\text{L mg}^{-1}$ ) and  $n$  are Freundlich constants which indicate the adsorption capacity and adsorption intensity, respectively. The plots of  $C_e/q_e$  against  $C_e$  and  $\log q_e$  against  $\log C_e$  for the Langmuir and Freundlich adsorption isotherms of Cu(II), Co(II) and Ni(II) by AFMNPECBs are shown in Fig. 9a and b, respectively.

For the determination of the feasibility of the adsorption process a dimensionless constant  $R_L$  is considered as an essential factor which is a characteristic of the Langmuir isotherm model and is given by eqn (9). The  $R_L$  value indicates favorable ( $0 < R_L < 1$ ), unfavorable ( $R_L > 1$ ), linear ( $R_L = 1$ ) or irreversible ( $R_L = 0$ ).

$$R_L = \frac{1}{1 + K_L C_0} \quad (9)$$

The results of the adsorption isotherms parameters for the metal ions are summarized in Table 2. The data presented in Table 2 clearly show that the adsorption equilibrium values well fitted with Freundlich model as  $R^2$  values for all three metal ions are much higher than that found in Langmuir model. The AFMNPECBs showed the maximum adsorption capacity ( $Q_m$ ) for the metal ions in an order  $\text{Cu(II)} > \text{Co(II)} > \text{Ni(II)}$  showing the values 172.4, 161.2, 103.0  $\text{mg g}^{-1}$ , respectively. These results are in agreement with the study reported by Monier *et al.*<sup>23</sup> The values of Langmuir constant  $R_L$  and Freundlich constant  $1/n$  for all the three metal ions were between 0–1 which supported the favorability of the adsorption process. However, the higher  $R^2$  values for all the metal ions in Freundlich model than in Langmuir model suggested multilayer adsorption on heterogeneous surface. The AFMNPECBs showed greater affinity for Cu(II) compare to Co(II) and Ni(II) ions as John–Teller effect is predominant for copper complexes.<sup>20,42</sup> Ghaee *et al.*<sup>43</sup> have also reported that chitosan showed higher adsorption capacity for Cu(II) removal than Ni(II) which is due to the stability of Cu(II) complex with chitosan. Vold *et al.* have reported that Cu(II) selectively adsorbed in chitosan in the presence of Ni(II), Zn(II) and Cd(II) ions.<sup>44</sup> Paulino *et al.* have also reported adsorption capacity of Cu(II) is higher than Pb(II) and Ni(II) ions because stability of the complex dominant among the certain metal ions.<sup>45</sup> A comparison of the adsorption capacities for studied metal ions on the AFMNPECBs and different types of adsorbents are summarized in Table 3. The AFMNPECBs showed far superior adsorption capacity as compared to other adsorbents which have been used for the removal of Cu(II), Co(II) and Ni(II) ions.

Table 2 Isotherm parameters for the adsorption of Cu(II), Co(II) and Ni(II) by AFMNPECBs under initial concentrations 100–500  $\text{mg L}^{-1}$ , contact time 160 min, adsorbent dose 10  $\text{g L}^{-1}$ , temperature 303 K and pH 6

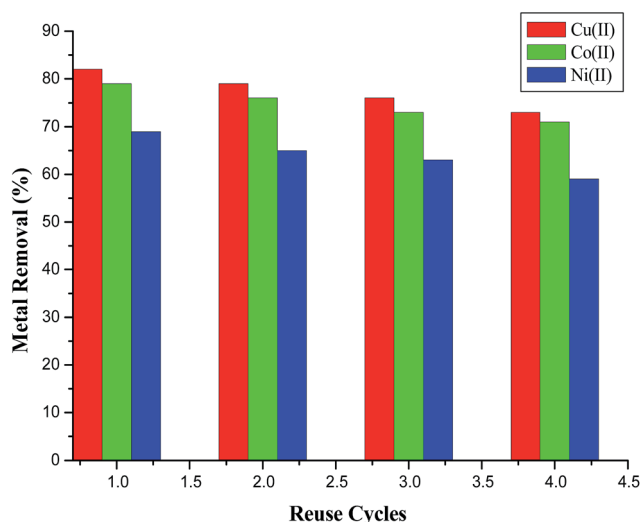
Isotherm models and parameters	Metals ions		
	Cu(II)	Co(II)	Ni(II)
<b>Langmuir model</b>			
$K_L \times 10^{-3}$ ( $\text{L mg}^{-1}$ )	4.152	3.362	1.821
$Q_m$ ( $\text{mg g}^{-1}$ )	172.4	161.2	103.0
$R_L$	0.706	0.748	0.846
$R^2$	0.603	0.437	0.520
<b>Freundlich model</b>			
$1/n$	0.861	0.901	0.854
$K_F$ ( $\text{L mg}^{-1}$ )	0.979	0.671	0.299
$R^2$	0.989	0.981	0.990





**Table 3** Comparison of the adsorption capacity of AFMNPECBs with various other adsorbents for the removal of Cu(II), Co(II) and Ni(II) ions

Adsorbents	$Q_m$ (mg g <sup>-1</sup> )			Reference
	Cu(II)	Co(II)	Ni(II)	
Chitosan-tripolyphosphate (CTPP) beads	26.0	—	—	46
Chitosan immobilized on bentonite	21.5	—	15.8	47
Cross-linked CS beads (glutaraldehyde)	2.58	1.68	2.34	48
CS <sub>4</sub> CPL <sub>1</sub> composite	11.3	24.20	7.94	49
Chitosan	16.8	—	2.4	50
Epichlorohydrin cross-linked chitosan	16.8	—	6.4	51
EDTA-modified chitosan	—	79.70	—	52
Cross-linked magnetic chitosan-isatin Schiff's base resin (CSIS)	103.1	53.51	40.15	53
AFMNPECBs	172.4	161.2	103.0	Present study

**Fig. 10** Reusability of AFMNPECBs using 0.1 M EDTA solution with repeat to reuse cycle and the percentage removal of the metal ions under the conditions given in Table 1.

### 3.6. Regeneration study

The stability and economic feasibility is an important parameter to the usability of the adsorbent. Thus, the regeneration of AFMNPECBs to restore the exhausted adsorption capacity of the adsorbent was studied using of 0.1 M EDTA solution. The AFMNPECBs were found to be effective and stable during the adsorption process where regeneration cycles were continued using 10 mL of 0.1 M EDTA solution. Fig. 10 shows that the fourth time of the adsorbent regeneration performed very well maintaining up to 70% of adsorption capacity which indicated that the reusability of AFMNPECBs was quite good.

## 4. Conclusion

The AFMNPECBs was successfully synthesized by modification and entrapment of MNPs which showed enhanced adsorption capacity due to increase in amino groups on its surface. The AFMNPECBs strongly followed Freundlich isotherm and pseudo second order kinetic models. The mechanism of

adsorption of the studied metal ions was due to complexation process. The adsorbent was easily recycled four time, by 0.1 M EDTA solution, maintaining the adsorption capacity upto 70%. The order of removal capacity by AFMNPECBs was Cu(II) > Co(II) > Ni(II). The results confirmed that entrapment of surface enhanced MNPs in polymer is highly effective, economical and efficient adsorbent for the removal of triple metal ions simultaneously.

## Conflicts of interest

There are no conflicts to declare.

## Acknowledgements

One of the authors (A. Asthana) is thankful to the University Grants Commission Regional Office, Bhopal, Madhya Pradesh, India, for sanction of a minor research project grant. S. Prasad is grateful to the University of the South Pacific, Suva, Fiji for support in various ways.

## References

- 1 M. Vandenbossche, M. Jimenez, M. Casetta and M. Traisnel, Remediation of heavy metals by biomolecules: A review, *Crit. Rev. Environ. Sci. Technol.*, 2015, **45**, 1644–1704.
- 2 B. Petrie, R. Barden and B. Kasprzyk-Hordern, A review on emerging contaminants in wastewaters and the environment: Current knowledge, understudied areas and recommendations for future monitoring, *Water Res.*, 2015, **72**, 3–27.
- 3 L. Yu, Y. Ma, C. N. Ong, J. Xie and Y. Liu, Rapid adsorption removal of arsenate by hydrous cerium oxide-graphene composite, *RSC Adv.*, 2015, **5**, 64983–64990.
- 4 M. W. Amer, R. A. Ahmad and A. M. Awwad, Biosorption of Cu(II), Ni(II), Zn(II) and Pb(II) ions from aqueous solution by *Sophora japonica* pods powder, *Int. J. Ind. Chem.*, 2015, **6**, 67–75.
- 5 Y. Wen, J. Ma, J. Chen, C. Shen, H. Li and W. Liu, Carbonaceous sulfur-containing chitosan-Fe(III): A novel adsorbent for efficient removal of copper(II) from water, *Chem. Eng. J.*, 2015, **259**, 372–380.



- 6 S. Hu, J. Song, F. Zhao, X. Meng and G. Wu, Highly sensitive and selective colorimetric naked-eye detection of  $\text{Cu}^{2+}$  in aqueous medium using a hydrazone chemosensor, *Sens. Actuators, B*, 2015, **215**, 241–248.
- 7 D. Borosova, A. Manova, J. Mocak and E. Beinrohr, Determination of nickel in hair samples by graphite furnace atomic absorption spectrometry and flow-through stripping chronopotentiometry, *Anal. Methods*, 2010, **2**, 1913–1917.
- 8 P. Z. Ray and H. J. Shipley, Inorganic nano-adsorbents for the removal of heavy metals and arsenic: A review, *RSC Adv.*, 2015, **5**, 29885–29907.
- 9 J. Wyszowska, J. Kucharski and E. Boros, Effect of nickel contamination on soil enzymatic activities, *Plant, Soil Environ.*, 2015, **51**, 523–531.
- 10 R. Lauwerys and D. Lison, Health risks associated with cobalt exposure—An overview, *Sci. Total Environ.*, 1994, **30**, 1–6.
- 11 U. K. Singh and B. Kumar, Pathways of heavy metals contamination and associated human health risk in Ajay River basin, India, *Chemosphere*, 2017, **174**, 183–199.
- 12 Y. Liu, C. N. Ong and J. Xie, Emerging nanotechnology for environmental applications, *Nanotechnol. Rev.*, 2016, **5**, 1–2.
- 13 M. R. Awual, M. Ismael and T. Yaita, Efficient detection and extraction of cobalt(II) from lithium ion batteries and wastewater by novel composite adsorbent, *Sens. Actuators, B*, 2014, **191**, 9–18.
- 14 S. Rengaraj and S. H. Moon, Kinetics of adsorption of Co(II) removal from water and wastewater by ion exchange resins, *Water Res.*, 2002, **36**, 1783–1793.
- 15 J. Tang, J. He, T. Liu and X. Xin, Removal of heavy metals with sequential sludge washing techniques using saponin: optimization conditions, kinetics, removal effectiveness, binding intensity, mobility and mechanism, *RSC Adv.*, 2017, **7**, 33385–33401.
- 16 M. Hua, S. Zhang, B. Pan, W. Zhang, L. Lv and Q. Zhang, Heavy metal removal from water/wastewater by nanosized metal oxides: A review, *J. Hazard. Mater.*, 2012, **211–212**, 317–331.
- 17 F. Ge, M. M. Li, H. Ye and B. X. Zhao, Effective removal of heavy metal ions  $\text{Cd}^{2+}$ ,  $\text{Zn}^{2+}$ ,  $\text{Pb}^{2+}$ ,  $\text{Cu}^{2+}$  from aqueous solution by polymer-modified magnetic nanoparticles, *J. Hazard. Mater.*, 2011, **211–212**, 366–372.
- 18 Y. Zhu, Y. Zheng, W. Wang and A. Wang, Highly efficient adsorption of Hg(II) and Pb(II) onto chitosan-based granular adsorbent containing thiourea groups, *J. Water Process. Eng.*, 2015, **7**, 218–226.
- 19 R. Verma, A. Asthana, A. K. Singh, S. Prasad and A. B. H. Susan, Novel glycine-functionalized magnetic nanoparticles entrapped calcium alginate beads for effective removal of lead, *Microchem. J.*, 2017, **130**, 168–178 and references cited therein.
- 20 L. Zhou, Y. Wang, Z. Liu and Q. Huang, Characteristics of equilibrium, kinetics studies for adsorption of Hg(II), Cu(II), and Ni(II) ions by thiourea-modified magnetic chitosan microspheres, *J. Hazard. Mater.*, 2009, **161**, 995–1002.
- 21 H. V. Tran, L. D. Tran and T. N. Nguyen, Preparation of chitosan/magnetite composite beads and their application for removal of Pb(II) and Ni(II) from aqueous solution, *Mater. Sci. Eng., C*, 2010, **30**, 304–310.
- 22 P. E. Podzus, M. V. Debandi and M. E. Daraio, Copper adsorption on magnetite-loaded chitosan microspheres: A kinetic and equilibrium study, *Phys. Rev. B: Condens. Matter Mater. Phys.*, 2012, **407**, 3131–3133.
- 23 M. Monier, D. M. Ayad, Y. Wei and A. A. Sarhan, Preparation and characterization of magnetic chelating resin based on chitosan for adsorption of Cu(II), Co(II) and Ni(II) ions, *React. Funct. Polym.*, 2010, **70**, 257–266.
- 24 S. P. Kuang, Z. Z. Wang, J. Liu and Z. C. Wu, Preparation of triethylenetetramine grafted magnetic chitosan for adsorption of Pb(II) ion from aqueous solutions, *J. Hazard. Mater.*, 2013, **260**, 210–219.
- 25 X. Song, C. Li, R. Xu and K. Wang, Molecular-ion-imprinted chitosan hydrogels for the selective adsorption of silver(I) in aqueous solution, *Ind. Eng. Chem. Res.*, 2012, **51**, 11261–11265.
- 26 L. Pontoni and M. Fabbicino, Use of chitosan and chitosan-derivatives to remove arsenic from aqueous solutions: A mini review, *Carbohydr. Res.*, 2012, **356**, 86–92.
- 27 Y. Pang, G. Zeng, L. Tang, Y. Zhang, Y. Liu, X. Lei, *et al.*, Preparation and application of stability enhanced magnetic nanoparticles for rapid removal of Cr(VI), *Chem. Eng. J.*, 2011, **175**, 222–227.
- 28 R. Antony, S. T. D. Manickam, K. Saravanan, K. Karuppasamy and S. Balakumar, Synthesis spectroscopic and catalytic studies of Cu(II), Co(II) and Ni(II) complexes immobilized on Schiff base modified chitosan, *J. Mol. Struct.*, 2013, **1050**, 53–60.
- 29 D. Liu, Z. Li, Y. Zhu, Z. Li and R. Kumar, Recycled chitosan nanofibril as an effective Cu(II), Pb(II) and Cd(II) ionic chelating agent: Adsorption and desorption performance, *Carbohydr. Polym.*, 2014, **111**, 469–476.
- 30 C. M. Futralan, C. C. Kan, M. L. Dalida, K. J. Hsien, C. Pascua and M. W. Wan, Comparative and competitive adsorption of copper, lead, and nickel using chitosan immobilized on bentonite, *Carbohydr. Polym.*, 2011, **83**, 528–536.
- 31 A. J. M. A. Karawi, Z. H. J. A. Qaisi, H. I. Abdullah, A. M. A. A. Mokaram and D. T. A. A. Heetimi, Synthesis, characterization of acrylamide grafted chitosan and its use in removal of copper(II) ions from water, *Carbohydr. Polym.*, 2011, **83**, 495–500.
- 32 Y. H. Yu, B. L. He and H. Q. Gu, Adsorption of bilirubin by amine-containing crosslinked chitosan resins, *Artif. Cells, Blood Substitutes, Immobilization Biotechnol.*, 2000, **28**, 307–320.
- 33 N. C. Feitoza, T. D. Goncalves, J. J. Mesquita, J. S. Meneguacci, M. K. M. S. Santos, J. A. Chaker, R. B. Cunha, A. M. M. Medeiros, J. C. Rubim and M. H. Sousa, Fabrication of glycine-functionalized maghemite nanoparticles form magnetic removal of copper from wastewater, *J. Hazard. Mater.*, 2014, **264**, 153–160.



- 34 C. Zhang, C. Shan, Y. Jin and M. Tong, Enhanced removal of trace arsenate by magnetic nanoparticles modified with arginine and lysine, *Chem. Eng. J.*, 2014, **254**, 340–348.
- 35 A. Dhillon, S. Prasad and D. Kumar, Recent advances and spectroscopic perspectives in fluoride removal, *Appl. Spectrosc. Rev.*, 2017, **52**, 175–230.
- 36 V. Chaudhary and S. Prasad, Rapid removal of fluoride from aqueous media using activated dolomite, *Anal. Methods*, 2015, **7**, 8304–8314 and references cited therein.
- 37 V. Tomar, S. Prasad and D. Kumar, Adsorptive removal of fluoride from aqueous media using *Citrus limonum* (Lemon) leaf, *Microchem. J.*, 2014, **112**, 97–103.
- 38 W. Fresenius, K. E. Quentin and W. Schneider, ed., *Water analysis: a practical guide to physico-chemical, chemical and microbiological water examination and quality assurance*, Springer Science & Business Media, 1988, vol. 373, 368, p. 380.
- 39 A. E. Nemr, Potential of pomegranate husk carbon for Cr(VI) removal from waste water: Kinetic and isotherm studies, *J. Hazard. Mater.*, 2009, **161**, 132–141.
- 40 F. C. Wu, R. L. Tseng and R. S. Juang, Initial behavior of intraparticle diffusion model used in the description of adsorption kinetics, *Chem. Eng. J.*, 2009, **153**, 1–8.
- 41 N. K. Amin, Removal of direct blue-106 dye from aqueous solution using new activated carbons developed from pomegranate peel: Adsorption equilibrium and kinetics, *J. Hazard. Mater.*, 2009, **165**, 52–62.
- 42 Y. Baba, K. Masaaki and Y. Kawano, Synthesis of a chitosan derivative recognizing planar metal ion and its selective adsorption equilibria of copper(II) over iron(III), *React. Funct. Polym.*, 1998, **36**, 167–172.
- 43 A. Ghaee, M. Shariaty-Niassar, J. Barzin and A. Zarghan, Adsorption of copper and nickel ions on macroporous chitosan membrane: Equilibrium study, *Appl. Surf. Sci.*, 2012, **258**, 7732–7743.
- 44 I. M. N. Vold, K. M. Varum, E. Guibal and O. Smidsrod, Bindings of ions to chitosan-selectivity studies, *Carbohydr. Polym.*, 2003, **54**, 471–477.
- 45 A. T. Paulino, F. A. Minasse, M. R. Guilherme, A. V. Reis, E. C. Muniz and J. Nozaki, Novel adsorbent based on silkworm chrysalides for removal of heavy metals from wastewaters, *J. Colloid Interface Sci.*, 2006, **301**, 479–487.
- 46 W. S. W. Ngah and S. Fatinathan, Adsorption characterization of Pb(II) and Cu(II) ions onto chitosan tripolyphosphate beads: Kinetic, equilibrium and thermodynamic studies, *J. Environ. Manage.*, 2010, **91**, 958–969.
- 47 C. M. Futralan, C. C. Kan, M. L. Dalida, K. J. Hsien, C. Pascua and M. W. Wan, Comparative and competitive adsorption of copper, lead, and nickel using chitosan immobilized on bentonite, *Carbohydr. Polym.*, 2011, **83**, 528–536.
- 48 Z. Cao, H. Ge and S. Lai, Studies on synthesis and adsorption properties of chitosan cross-linked by glutaraldehyde and Cu(II) as template under micro wave irradiation, *Eur. Polym. J.*, 2001, **37**, 2141–2143.
- 49 M. V. Dinu and E. S. Dragan, Evaluation of Cu<sup>2+</sup>, Co<sup>2+</sup> and Ni<sup>2+</sup> ions removal from aqueous solution using a novel chitosan/clinoptilolite composite: Kinetics and isotherms, *Chem. Eng. J.*, 2010, **160**, 157–163.
- 50 C. Huang, Y. C. Chung and M. R. Liou, Adsorption of Cu(II) and Ni(II) by pelletized biopolymer, *J. Hazard. Mater.*, 1996, **45**, 265–277.
- 51 S. Tan, Y. Wang, C. Peng and Y. Tang, Synthesis and adsorption properties for metal ions of cross linked chitosan acetate crown ethers, *J. Appl. Polym. Sci.*, 1999, **71**, 2069–2074.
- 52 E. Repo, R. Koivula, R. Harjula and M. Sillanpaa, Effect of EDTA and some other interfering species on the adsorption of Co(II) by EDTA modified chitosan, *Desalination*, 2013, **321**, 93–102.
- 53 M. Monier, D. M. Ayad, Y. Wei and A. A. Sarhan, Adsorption of Cu(II), Co(II) and Ni(II) ions by modified magnetic chitosan chelating resin, *J. Hazard. Mater.*, 2010, **177**, 962–970.

